Empirical Models for Dark Matter Halos. I. Model Comparison

David Merritt
Department of Physics, Rochester Institute of Technology, Rochester, NY 14623, USA.

Alister W. Graham
Mount Stromlo and Siding Spring Observatories, Australian National University, Private Bag, Weston Creek PO, ACT 2611, Australia.

Ben Moore
University of Zurich, Winterthurerstrasse 190, CH-8057, Zürich, Switzerland.

Jürg Diemand
Department of Astronomy and Astrophysics, University of California, 1156 High Street, Santa Cruz, CA 95064, USA.

Balša Terzić
Department of Physics, Northern Illinois University, DeKalb, IL 60115, USA.

ABSTRACT

We use techniques from nonparametric function estimation theory to extract the density profiles, and their derivatives, from a set of N-body dark matter halos. We also compare our nonparametric estimates of $\rho(r)$ with a variety of parametric models to determine which provide the best fit. We consider N-body halos generated from (i) ΛCDM simulations of gravitational clustering, and (ii) isolated, spherical collapses. The 3-parameter models we consider include a double power-law model (an NFW-like model with arbitrary inner power-law slope γ), Dehnen & McLaughlin's anisotropic model, Sérsic's function (traditionally applied to projected light profiles), and the density model of Prugniel & Simien that was designed to match the deprojected form of Sérsic's $R^{1/n}$ model and which is applied here for the first time to dark matter halos. Perhaps not surprisingly, these models provide a better description of the data than the 2-parameter NFW and Burkert models. Overall, the best-fitting model is Sérsic's, although the Prugniel-Simien model performs slightly better for the cluster-sized ΛCDM halos, and the Dehnen-McLaughlin model performs best for the galaxy-sized ΛCDM halos. With regard to the spherical collapse halos, both the Prugniel-Simien and Sérsic $r^{1/n}$ models describe the density distributions well, with an rms scatter some four times smaller than that obtained with either the NFW-like model or the 3-parameter Dehnen-McLaughlin model. Finally, we confirm recent claims of a systematic variation in profile shape with halo mass.

Subject headings: dark matter — galaxies: halos — methods: N-body simulations

1. Introduction

Early work on the self-similar collapse of (spherical) primordial over-densities resulted in virial-

ized structures having density profiles described by a single power-law (e.g., Fillmore & Goldreich 1984; Bertschinger 1985; Hoffman 1988). As N-body simulations improved, the logarithmic profile slopes of cold dark matter (CDM) halos, simulated in hierarchical merger models, were observed not to remain constant, but to steepen with increasing radius (e.g., West, Dekel & Oemler 1987; Frenk et al. 1988; Efstathiou et al. 1988).

Dubinski & Carlberg (1991) adopted Hernquist's (1990) double power-law model to describe these density profiles with continuously changing slope. This empirical model, a variant of the Jaffe (1983) model, has an inner logarithmic slope of -1 and an outer logarithmic slope of -4. It was introduced as an analytical approximation to the deprojected form of de Vaucouleurs' $R^{1/4}$ light-profile. Navarro, Frenk, & White (1995) modified this to give the so-called NFW model that has an outer logarithmic slope of -3 rather than -4, while Moore et al. (1998, 1999) suggested that a further variation having an inner logarithmic slope of -1.4 or -1.5 may be more appropriate.

Recently, Navarro et al. (2004) have (unknowingly) applied Sérsic's (1963, 1968) function to the density profiles of their dark matter halos. This flexible, 3-parameter function was independently developed for describing density profiles, as opposed to (projected) light profiles, by Einasto (1965, 1968, 1969; see also Einasto & Haud 1989). We will therefore at times refer to this function, when applied to density profiles, as Einasto's $r^{1/n}$ model, to help distinguish it from Sérsic's $R^{1/n}$ model. Navarro et al. (2004) found that this model provided a comparable and often better description of the data than an NFW-like, double power-law model with a variable inner, logarithmic slope γ (see also Merritt et al. 2005 and Diemand, Moore, & Stadel 2004b, their Table 3).

Although the double power-law model and Sérsic's law are simply empirical fitting functions (but see Binney 1982, Merritt et al. 1989, Ciotti 1991, and Márquez et al. 2001 for physical motivations), a more unified scheme would involve the application of Sérsic's $R^{1/n}$ model to projected (on the plane of the sky) distributions, and the use of some other expression for the 3-dimensional, spatial profiles. Indeed, not only do elliptical galaxies have Sérsic $R^{1/n}$ light profiles (e.g., Caon, Capaccioli, & D'Onofrio 1993; Graham & Guzmán 2003, and references therein), but Demarco et al. (2003) have observed that the hot gas in galaxy clusters also has a (projected) Sérsic distribution. Moreover, Merritt et al. (2005) revealed that the (numerically) deprojected form of the Sérsic $R^{1/n}$ model performs equally as well as the direct application of the Einasto $r^{1/n}$ model to the N-body haloes.

In what follows, we therefore explore the applicability of Prugniel & Simien's (1997) analytical, 3-parameter, density model that was developed to approximate the *de*projected form of the Sérsic $R^{1/n}$ light-profile. Apart from the work of Lima Neto et al. (1999), Pignatelli & Galletta (1999), and Márquez et al. (2000, 2001), the Prugniel-Simien model has received little attention to date. Demarco et al. (2003) have however applied it to the gas density profiles of 24 galaxy clusters observed with ROSAT, and Terzić & Graham (2005) showed that it provided a superior description of the density profiles of real elliptical galaxies compared with either the Jaffe or Hernquist models. As far as we are aware, ours is the first application of the Prugniel-Simien model to N-body halos.

In Section 2 we introduce the data sets to be analyzed. These consist of N-body simulations of ten ΛCDM halos and two halos formed by monolithic collapse that also experienced a rapid and violent (although nearly spherically-symmetric) restructuring of the initial system. Historically, some of the first N-body simulations were simple cold collapse calculations like these (e.g. van Albada 1961; Aarseth 1963; Hénon 1964; Peebles 1970). It was quickly realized that, given appropriately low but non-zero levels of initial random velocity, the end state of such systems resembled the $R^{1/4}$ profiles observed in elliptical galaxies (e.g. van Albada 1982; Aguilar & Merritt 1990). The similarity between the end state of cold collapse simulations and hierarchical CDM models has been discussed in Moore et al. (1999). A closer re-inspection of the data, however, (e.g. Figure 4–6 in van Albada 1982) reveals obvious and systematic deviations from the $R^{1/4}$ model in the cold collapses. From a visual inspection of these figures, one can see that the distributions would be better described with an $R^{1/n}$ profile having $n < 4$, consistent with what we find here.

In Section 3 we present the nonparametric method used to construct the density profiles and

their logarithmic slopes. In addition to three 2-parameter models (NFW, Burkert, isotropic Dehnen-McLaughlin), Section 4 presents four 3-parameter models (a double power-law, the anisotropic Dehnen-McLaughlin model, Einasto's $r^{1/n}$ model, and the Prugniel-Simien model) and their application to our (unprojected) dark halo density profiles. How well these empirical models perform is reported in Section 5 and our findings are summarized in Section 6.

In Graham et al. (2006a, hereafter Paper II), we explore the Einasto and Prugniel-Simien models in more detail. Specifically, we explore the logarithmic slope of these models and compare the results with observations of real galaxies. We also present the models' circular velocity profiles and their ρ/σ^3 profiles. Helpful expressions for the concentration and assorted scale radii: $r_s, r_{-2}, r_{\rm e}, R_{\rm e}, r_{\rm vir}$, and $r_{\rm max}$ — the radius where the circular velocity profile has its maximum value — are also derived. Because the Prugniel-Simien model yields the same parameters as those coming from Sérsic-model fits, we are able to show in a third paper (Graham et al. 2006b, hereafter Paper III) the location of our dark matter halos on the Kormendy diagram ($\mu_{\rm e}$ vs. $\log R_{\rm e}$), along with real galaxies. We additionally show in Paper III the location of our dark matter halos and real galaxies and clusters in a new $\log(\rho_{\rm e}) - \log(R_{\rm e})$ diagram.

2. Data: Dark matter halos

We use a sample of relaxed, dark matter halos from Diemand, Moore, & Stadel (2004a,b). Details about the simulations, convergence tests, and an estimate of the converged scales can be found in those papers. Briefly, the sample consists of six, cluster-sized halos (models: A09, B09, C09, D12, E09, and F09) resolved with 5 to 25 million particles within the virial radius, and four, galaxy-sized halos (models: G00, G01, G02, and G03) resolved with 2 to 4 million particles. The innermost resolved radii are 0.3% to 0.8% of the virial radius, $r_{\rm vir}$. The outermost data point is roughly at the virial radius, which is defined in such a way that the mean density within $r_{\rm vir}$ is $178\Omega_M^{0.45}\rho_{\rm crit} = 98.4\rho_{\rm crit}$ using $\Omega_m = 0.268$ (Eke, Cole, & Frenk 1996; Spergel et al. 2003). The virial radius thus encloses an overdensity which is 368 times denser than the mean matter density. We adopted the same estimates of the halo centers as in the Diemand et al. papers; these were computed using SKID (Stadel 2001), a kernel-based routine.

In an effort to study the similarities between cold, collisionless collapse halos and CDM halos, we performed two additional simulations. We distributed 10^7 particles with an initial density profile $\rho(r) \propto r^{-1}$, within a unit radius sphere with total mass 1 (M11) and 0.1 (M35). The particles have zero kinetic energy and the gravitational softening was set to 0.001. Each system collapsed and underwent a radial-orbit instability (Merritt & Aguilar 1985) which resulted in a virialized, triaxial/prolate structure. The lower mass halo, M35, collapsed less violently over a longer period of time.

3. Nonparametric estimation of density profiles and their derivatives

Density profiles of N-body halos are commonly constructed by counting particles in bins. While a binned histogram is a non-parametric function estimate of the "real" density profile, such an estimate does of course vary with the chosen size and location of the binar, and can, at times, have rather undesirable bias properties (see, e.g., Stepanas & Saha 1995). A better approach is to view the particle positions as a random sample drawn from some unknown, smooth density $\rho(\mathbf{r})$, and to use techniques from nonparametric function estimation to construct an estimate of ρ (e.g., Scott 1992). Such techniques often have the property that the density estimate, $\hat{\rho}(\mathbf{r})$, is a smooth, differentiable function, hence quantities like the logarithmic derivative can be computed via direct differentiation of $\hat{\rho}$. In the limit that the "sample size" N tends to infinity, these estimates exactly reproduce the density function from which the data were drawn, as well as many properties of that function, e.g. its derivatives (Silverman 1986).

We used a kernel-based algorithm for estimating $\rho(r)$, similar to the algorithms described in Merritt & Tremblay (1994), Merritt (1996), and Reed et al. (2005). The starting point is an estimate of the 3D density obtained by replacing each particle at position $\mathbf{r}_i$ by a kernel of width h_i, and

summing the kernel densities:

$$\hat{\rho}(\mathbf{r}) = \sum_{i=1}^{N} \frac{m_i}{h_i^3} K\left[\frac{1}{h_i}\left|\mathbf{r}-\mathbf{r}_i\right|\right]. \quad (1)$$

Here m_i is the mass associated with the ith particle and K is a normalized kernel function, i.e. a density function with unit volume. We adopted the Gaussian kernel,

$$K(y) = \frac{1}{(2\pi)^{3/2}} \mathrm{e}^{-y^2/2}. \quad (2)$$

The density estimate of equation (1) has no imposed symmetries. We now suppose that $\rho(\mathbf{r}) = \rho(r)$, i.e. that the underlying density is spherically symmetric about the origin. In order that the density estimate have this property, we assume that each particle is smeared uniformly around the surface of the sphere whose radius is r_i. The spherically-symmetrized density estimate is

$$\hat{\rho}(r) = \sum_{i=1}^{N} \frac{m_i}{h_i^3} \frac{1}{4\pi} \int d\phi \int d\theta \ \sin\theta \ K\left(\frac{\mathrm{d}}{h_i}\right) \quad (3a)$$

$$\mathrm{d}^2 = \left|\mathbf{r}-\mathbf{r}_i\right|^2 \quad (3b)$$

$$= r_i^2 + r^2 - 2rr_i\cos\theta \quad (3c)$$

where θ is defined (arbitrarily) from the $\mathbf{r}_i$-axis. This may be expressed in terms of the angle-averaged kernel $\tilde{K}$,

$$\tilde{K}(r, r_i, h_i) \equiv \frac{1}{4\pi} \int_{-\pi/2}^{\pi/2} d\phi \times \int_0^{2\pi} d\theta \ \sin\theta \ K\left(h_i{}^{-1}\sqrt{r_i^2 + r^2 - 2rr_i\cos\theta}\right) \quad (4a)$$

$$= \frac{1}{2}\int_{-1}^{1} d\mu \ K\left(h_i{}^{-1}\sqrt{r_i^2 + r^2 - 2rr_i\mu}\right), \quad (4b)$$

as

$$\hat{\rho}(r) = \sum_{i=1}^{N} \frac{m_i}{h_i^3} \tilde{K}(r, r_i, h_i). \quad (5)$$

Substituting for the Gaussian kernel, we find

$$\tilde{K}(r, r_i, h_i) = \frac{1}{(2\pi)^{3/2}} \left(\frac{rr_i}{h_i^2}\right)^{-1} \times \exp\left[-(r_i^2 + r^2)/2h_i^2\right] \sinh(rr_i/h_i^2). \quad (6)$$

A computationally preferable form is

$$\tilde{K} = \frac{1}{2(2\pi)^{3/2}} \left(\frac{rr_i}{h_i^2}\right)^{-1} \times \left\{\exp\left[-(r_i - r)^2/2h_i^2\right] - \exp\left[-(r_i + r)^2/2h_i^2\right]\right\} \quad (7)$$

Equations (5) and (7) define the density estimate. Typically, one sets up a grid in radius and evaluates $\hat{\rho}(r)$ discretely on the grid. However we stress that the density estimate itself is a continuous function and is defined independently of any grid.

Given a sample of N positions and particle masses drawn randomly from some (unknown) $\rho(r)$, the goal is to construct an estimate $\hat{\rho}(r)$ that is as close as possible, in some sense, to $\rho(r)$. In the scheme just described, one has the freedom to adjust the N kernel widths h_i in order to achieve this. In general, if the h_i are too small, the density estimate will be "noisy," i.e. $\hat{\rho}(r)$ will exhibit a large *variance* with respect to the true density; while if the h_i are too large, the density estimate will be over-smoothed, i.e. there will be a large *bias*. (Of course the same is true for binned histograms, although in general the bias-variance tradeoff for histograms is less good than for kernel estimates.) If the true $\rho(r)$ were known *a priori*, one could adjust the h_i so as to minimize (say) the mean square deviation between $\rho(r)$ and $\hat{\rho}(r)$. Since $\rho(r)$ is not known *a priori* for our halos, some algorithm must be adopted for choosing the h_i. We followed the standard practice (e.g. Silverman 1986, p.101) of varying the h_i as a power of the local density:

$$h_i = h_0 \left[\hat{\rho}_{\mathrm{pilot}}(r_i)/g\right]^{-\alpha}, \quad (8)$$

where $\hat{\rho}_{\mathrm{pilot}}(r)$ is a "pilot" estimate of $\rho(r)$, and g is the geometric mean of the pilot densities at the r_i. Since the pilot estimate is used only for assigning the h_i, it need not be differentiable, and we constructed it using a nearest-neighbor scheme.

The final density estimate $\hat{\rho}(r)$ is then a function of two quantities: h_0 and α. Figure 1 illustrates the dependence of $\hat{\rho}(r)$ on h_0 when the kernel algorithm is applied to a random sample of 10^6 equal-mass particles generated from an Einasto density profile with $n = 5$, corresponding to typical values observed in Merritt et al. (2005). Each of the density profile estimates of Figure 1 used $\alpha = 0.3$. As expected, for small h_0, the estimate of $\rho(r)$ is noisy, but faithful in an average way to the true profile; while for large h_0, $\rho(r)$ is a smooth function but is biased at small radii due to the averaging effect of the kernel. The "optimum" h_0 for this sample is $\sim 0.05\, r_{\mathrm{e}}$.

In what follows, we will compare the nonparametric estimates $\hat{\rho}(r)$ derived from the N-body

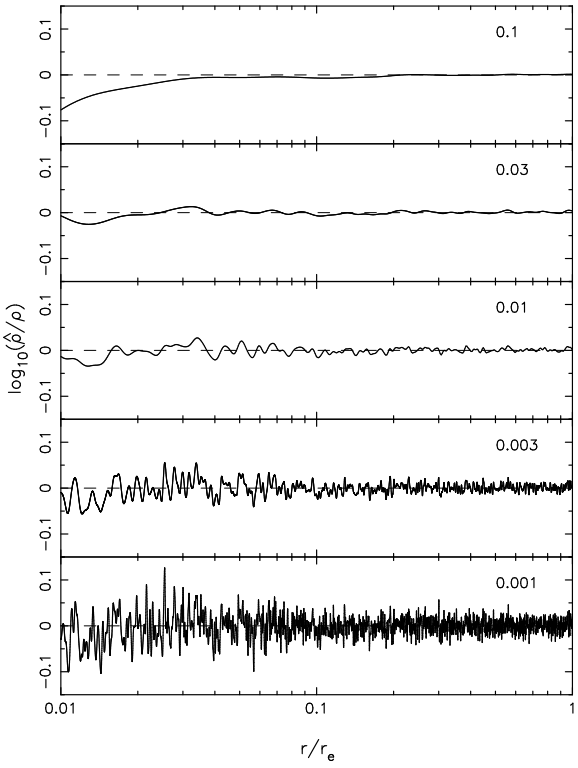

Fig. 1.— Nonparametric, bias-variance tradeoff in the estimation of $\rho(r)$ using a single sample of 10^6 radii generated from a halo having an Einasto $r^{1/n}$ density profile with $n = 5$ (see Section 4.2). From top to bottom, $h_0 = (0.1, 0.03, 0.01, 0.003, 0.001)\, r_e$; all estimates used $\alpha = 0.3$ (see equations 5, 7, and 8).

models with various parametric fitting functions, in order to find the best-fitting parameters of the latter by minimizing the rms residuals between the two profiles. For this purpose, any of the density estimates in Figure 1 would yield similar results, excepting perhaps the density estimate in the uppermost panel which is clearly biased at small radii. In addition, we will also wish to characterize the rms value of the deviation between the "true" profile and the best-fitting parametric models. Here it is useful for the kernel widths to be chosen such that the residuals are dominated by the systematic differences between the parametric and nonparametric profiles, and not by noise in $\hat{\rho}(r)$ resulting from overly-small kernels. We verified that this condition was easily satisfied for all of the N-body models analyzed here: there was always found to be a wide range of (h_0, α) values such that the residuals between $\hat{\rho}(r)$ and the parametric function were nearly constant. This is a consequence of the large particle numbers ($> 10^6$) in the N-body models, which imply a low variance even for small h_0.

As discussed above, quantities like the derivative of the density can also be computed directly from $\hat{\rho}(r)$. Figure 2 shows nonparametric estimates of the slope, $d\log\rho/d\log r$, for the same 10^6 particle data set as in Figure 1. We computed derivatives simply by numerically differentiating $\hat{\rho}(r)$; alternatively, we could have differentiated equation (7). Figure 2 shows that as h_0 is increased, the variance in the estimated slope drops, and for $h_0 \approx 0.2\, r_e$ the estimate is very close to the true function. We note that the optimal choice of h_0 when estimating derivatives is larger than when estimating $\rho(r)$ ($\sim 0.2\, r_e$ vs. $\sim 0.05\, r_e$); this is a well-known consequence of the increase in "noise" associated with differentiation. Figure 2 also illustrates the important point that there is no need to impose an additional level of smoothing when computing the density derivatives (as was done, e.g., in Reed et al. 2005); it is sufficient to increase h_0.

3.1. Our density profiles

Figure 3 shows, using $\alpha = 0.3$ and $h_0 = 0.05\, r_e$ (left panel) and $\alpha = 0.4$ and $h_0 = 0.05\, r_e$ (right panel), the nonparametric estimates of $\rho(r)$ (left panel) and $\gamma(r) \equiv d\log\rho/d\log r$ (right panel) for the ten N-body halos. Figure 4 shows the same

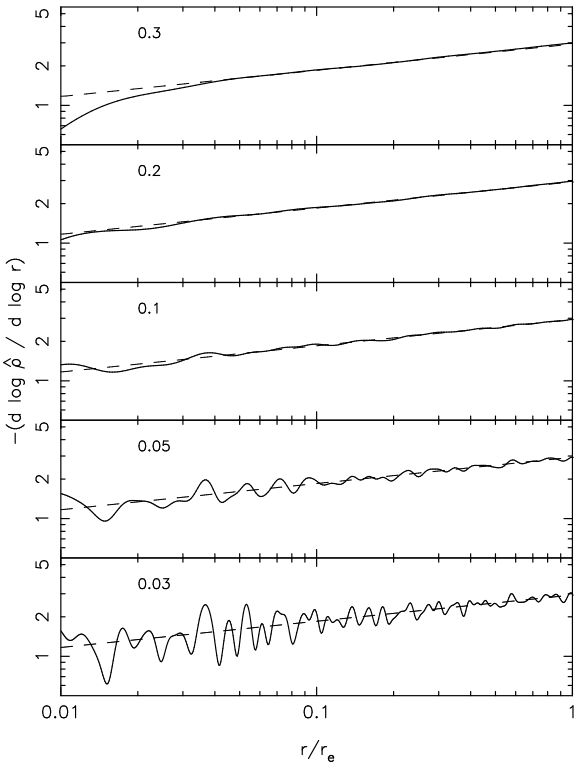

Fig. 2.— Five estimates of the logarithmic slope of an Einasto $r^{1/n}$ halo, derived via differentiation of $\hat{\rho}(r)$. The same sample of 10^6 radii was used as in Figure 1. From top to bottom, $h_0 = (0.3, 0.2, 0.1, 0.05, 0.03)\, r_{\rm e}$; each estimate used $\alpha = 0.4$ (see equation 8). Dashed lines show the true slope.

quantities for the two data sets generated from cold collapses. We stress that these plots – especially, the derivative plots – could not have been made from tables of binned particle numbers. For most profiles, the slope is a rather continuous function of radius and does not appear to reach any obvious, asymptotic, central value by $\sim 0.01 r_{\rm vir}$. Instead, $\hat{\gamma}(r)$ varies approximately as a power of r, i.e. $\log\hat{\gamma}$ vs. $\log r$ is approximately a straight line. Accordingly, we have fitted straight lines, via a least-squares minimization, to the logarithmic profile slopes in the right-hand panels of Figures 3 and 4. The regression coefficients, i.e. slopes, are inset in each panel. (These slope estimates should be seen as indicative only; they are superseded by the model fits discussed below.) In passing we note that such a power-law dependence of γ on r is characteristic of the Einasto model, with the logarithmic slope equal to the exponent $1/n$. Noise and probable (small) deviations from a perfect Einasto $r^{1/n}$ model are expected to produce slightly different exponents when we fit the density profiles in the following Section with Einasto's $r^{1/n}$ model and a number of other empirical functions.

On average, the slope at $r_{\rm vir}$ is around -3, but there are large fluctuations and some halos reach a value of -4, as previously noted in Diemand et al. (2004b). The reason for these fluctuation may be because the outer parts are dynamically very young (i.e. measured in local dynamical times) and they have only partially completed the violent relaxation into a stable, stationary equilibrium configuration. We are not able to say with any confidence what the slopes do beyond $r_{\rm vir}$.

4. Empirical models

In this section, we present four parametric density models, each having three independent parameters: two "scaling" parameters and one "shape" parameter. We measured the quality of each parametric model's fit to the nonparametric $\hat{\rho}(r)$'s using a standard metric, the integrated square deviation:

$$\int d\,(\log r)\,[\log\hat{\rho}(r) - \log\rho_{\rm param}(r)]^2 \qquad (9)$$

where $\rho_{\rm param}$ is understood to depend on the various fitting parameters as well as on r. We chose

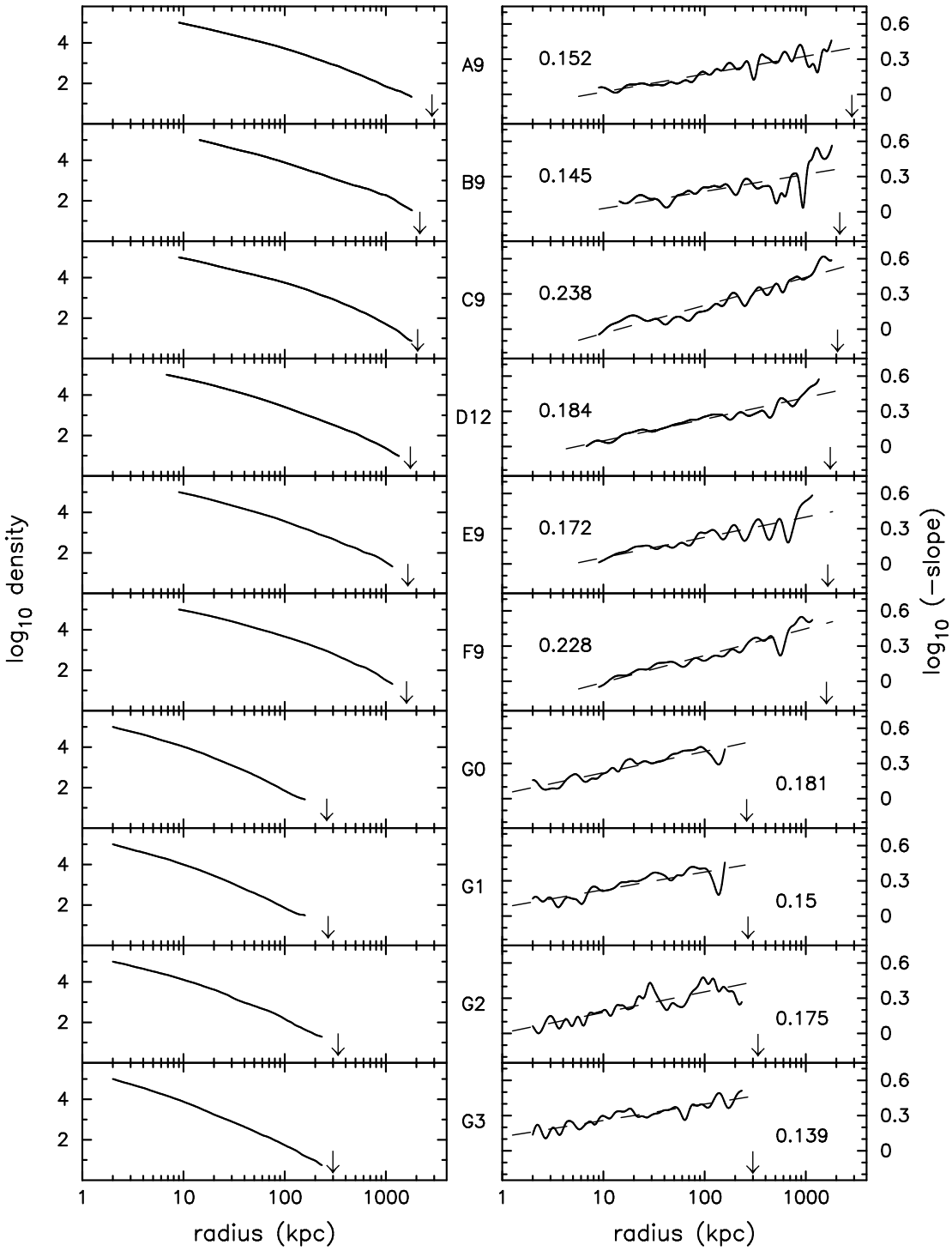

Fig. 3.— Nonparametric estimates of the density $\rho(r)$ (left panel) and the slope $d\log\rho/d\log r$ (right panel) for the ten N-body halos of Table 1. The virial radius r_{vir} is marked with an arrow. Dashed lines in the right hand panels are linear fits of $\log(-d\log\rho/d\log r)$ to $\log r$; regression coefficients are also given.

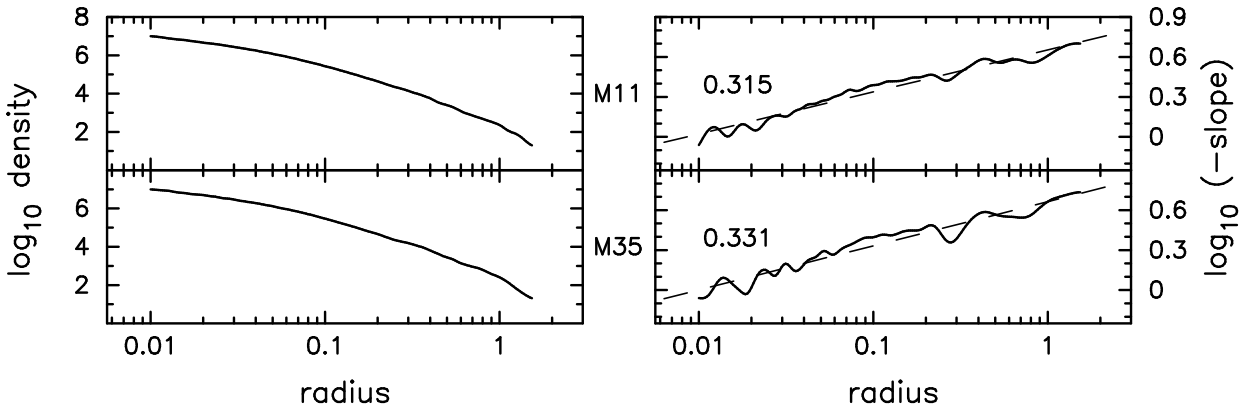

Fig. 4.— Nonparametric estimates of $\rho(r)$ (left panel) and $d\log\rho/d\log r$ (right panel) for the two "collapse" models. Dashed lines in the right hand panels are linear fits of $\log(-d\log\rho/d\log r)$ to $\log r$.

to evaluate this integral by discrete summation on a grid spaced uniformly in $\log r$; our measure of goodness-of-fit (which was also the quantity that was minimized in determing the best-fit parameters) was

$$\Delta^2 \equiv \frac{\sum_{j=1}^{m}\delta_j^2}{m-3}, \quad (10a)$$

$$\delta_j = \log_{10}[\hat{\rho}(r_j)/\rho_{\rm param}(r_j)] \quad (10b)$$

with $m = 300$. With such a large value of m the results obtained by minimizing (10a) and (9) are indistinguishable. We note that the quantity Δ^2 in equation (10a) is reminiscent of the standard χ^2, but the resemblance is superficial. For instance, Δ^2 as defined here is independent of m in the large-m limit (and our choice of $m = 300$ puts us effectively in this limit). Furthermore there is no binning involved in the computation of Δ^2; the grid is simply a numerical device used in the computation of (9).

(We also note here one very nice feature of nonparametric density estimates: namely, their flexibility. Not only do they constitute (i) "standalone" representations of $\rho(r)$ and $\gamma(r)$, as in Figures 3 and 4. They are also well-suited to (ii) inferring best-fit values for the fitting parameters of parametric functions, by minimizing equation (9); and (iii) comparing the goodness-of-fit of different parametric functions, via the relative values of Δ^2. Competing techniques exist for (ii) and/or (iii) but (as far as we are aware) not for all three. For instance, the standard technique of computing binned densities can give good results for (ii) and (iii) but not (i). Sarazin's (1980) maximum-likelihood algorithm provides a more direct route to (ii) but is not appropriate for (i) or (iii), etc.)

4.1. Double power-law models

Hernquist (1990, his equation 43) presented a 5-parameter generalization of Jaffe's (1983) double power-law model. Often referred to as the (α,β,γ) model, it can be written as

$$\rho(r) = \rho_s 2^{(\beta-\gamma)/\alpha}\left(\frac{r}{r_s}\right)^{-\gamma}\left[1+\left(\frac{r}{r_s}\right)^{\alpha}\right]^{(\gamma-\beta)/\alpha}, \quad (11)$$

where ρ_s is the density at the scale radius, r_s, which marks the center of the transition region between the inner and outer power-laws having slopes of $-\gamma$ and $-\beta$, respectively. The parameter α controls the sharpness of the transition (see Zhao et al. 1996; Kravtsov et al. 1998; and equations (37) and (40b) in Dehnen & McLaughlin 2005). Setting (α,β,γ)=(1, 3, 1) yields the NFW model, while (1.5, 3, 1.5) gives the model in Moore et al. (1999). Other combinations have been used, for example, (1,3,1.5) was applied in Jing & Suto (2000) and (1,2.5,1) was used by Rasia, Tormen, & Moscardini (2004).

In fitting dark matter halos, Klypin et al. (2001, their figure 8) have noted a certain degree of degeneracy when all of the 5 paramaters are allowed to vary. Graham et al. (2003, their figures 3 and 4) have also observed the parameters of this empirical model to be highly unstable when applied to (light) profiles having a continuously changing

logarithmic slope. Under such circumstances, the parameters can be a strong function of the fitted radial extent, rather than reflecting the intrinsic physical properties of the profile under study. This was found to the case when applied to the dark matter halos under study here. We have therefore chosen to constrain two of the model parameters, holding α fixed at 1 and β fixed at 3.

In recent years, as the resolution in N-body simulations has improved, Moore and collaborators have found that the innermost (resolved) logarithmic slope of dark matter halos has a range of values which are typically shallower than -1.5: recently obtaining a mean value ($\pm$ standard deviation) equal to -1.26 ± 0.17 at 1% of the virial radius (Diemand, Moore, & Stadel 2004b). At the same time, Navarro et al. (2004) report that the NFW model underestimates the density over the inner regions of most of their halos, which have innermost resolved slopes ranging from -1.6 to -0.95 (their Figure 3). A model with an outer slope of -3 and an inner slope of $-\gamma$ might therefore be more appropriate. Such a model has been used before and can be written as

$$\rho(r) = \frac{2^{3-\gamma}\rho_s}{(r/r_s)^{\gamma}(1+r/r_s)^{3-\gamma}}. \qquad (12)$$

The total mass of this model is infinite however.

We have applied the above (1, 3, γ) model to our dark matter density profiles, the results of which are shown in Figure 5 for the N-body halos, and in the upper panel of Figure 6 for the cold collapse models. Similar results were obtained by Diemand et al. (2004b) who fitted the N-body data after it was binned into spherical (and also triaxial) shells. The rms scatter, Δ, is inset in each figure and additionally reported in Table 1.

4.1.1. Two-parameter models

Recognizing that galaxies appear to have flat inner density profiles (e.g., Flores & Primack 1994; Moore 1994), Burkert (1995) cleverly introduced a density model having an inner slope of zero and an outer profile that decayed as r^{-3}. His model is given by the expression

$$\rho(r) = \frac{\rho_0 {r_s}^3}{(r+r_s)(r^2+{r_s}^2)}, \qquad (13)$$

where ρ_0 is the central density and r_s is a scale radius. Application of this model in Figure 7 reveals that, with only 2 free parameters, it does not provide as good a fit to the simulated dark matter halos as the (1, 3, γ) model presented above. The hump-shaped residual profiles in Figure 7 signify the model's inability to match the curvature of our density profiles.

It is however worth pointing out that this flat core model was developed to fit the observed rotation curves in low surface brightness galaxies, after the contribution from the baryonic component had been subtracted out. Given that it appears to perform this task well, but doesn't match the simulated dark matter halos, may suggest a problem with the hierarchical ΛCDM and cold collapse models.

As noted previously, the NFW (α, β, γ)=(1, 3, 1) model also has only two parameters: ρ_s and r_s. Because this model is still often used, we apply it to our halos in Figure 8. Comparison with Figure 5 reveals that the NFW model never performs better than the (1, 3, γ) model; the residuals are $\sim$50% larger and sometimes twice as large. Importantly, the large-scale curvature observed in many of the NFW resdiual profiles (Figure 8) reveals that this model does not describe the majority of the halos, and that the (1, 3, γ) model should be preferred over the NFW model.

An alternative 2-parameter expression has recently been studied by Dehnen & McLaughlin (2005, their equation (20b); see also Austin et al. 2005). It is a special case of a more general family of models — which we test next — when the velocity ellipsoid at the halo centre is isotropic and $\rho/{\sigma_r}^3$ is a (special) power law in radius, varying as $r^{-35/18}$. This 2-parameter density model is an $(\alpha, \beta, \gamma) = (4/9, 31/9, 7/9)$ model given by

$$\rho(r) = \frac{2^6\rho_s}{(r/r_s)^{7/9}[1+(r/r_s)^{4/9}]^6}, \qquad (14)$$

and is applied in Figure 9. It clearly provides a much better match to the dark matter halo density profiles in comparison with the previous 2-parameter model over the fitted radial range, but the rms scatter reveals that it does not perform as well as the (1, 3, γ) model, nor can it describe the 'spherical collapse' halos (Figure 6). We therefore, in the following subsection, test the more general 3-parameter model given in Dehnen & McLaughlin (2005).

TABLE 1
THREE PARAMETER MODELS

Halo Id.	r_s kpc	$\log \rho_s$ $M_\odot$ pc^{-3}	γ	Δ dex	$r_{\rm e}$ kpc	$\log \rho_e$ $M_\odot$ pc^{-3}	$n_{\rm Ein}$	Δ dex	$R_{\rm e}$ kpc	$\log \rho'$ $M_\odot$ pc^{-3}	$n_{\rm PS}$	Δ dex
		(1,3,γ)				Einasto $r^{1/n}$				Prugniel-Simien		
					Cluster-sized halos							
A09	626.9	−3.87	1.174	0.025	5962.	−6.29	6.007	**0.015**	2329.	−2.73	3.015	0.021
B09	1164.	−4.75	1.304	**0.037**	17380.	−7.66	7.394	0.041	4730.	−3.34	3.473	0.038
C09	241.8	−3.27	0.896	0.040	1247.	−4.95	3.870	0.030	738.9	−2.55	2.192	**0.016**
D12	356.1	−3.82	1.251	0.026	2663.	−6.02	5.939	0.020	1232.	−2.52	3.147	**0.019**
E09	382.5	−3.96	1.265	0.033	2611.	−6.06	5.801	0.032	1231.	−2.62	3.096	**0.030**
F09	233.9	−3.51	1.012	0.030	1235.	−5.26	4.280	0.025	697.3	−2.63	2.400	**0.017**
					Galaxy-sized halos							
G00	27.96	−3.16	1.163	**0.020**	189.0	−5.22	5.284	0.023	114.4	−2.02	3.135	0.028
G01	35.34	−3.36	1.275	0.029	252.6	−5.51	5.873	**0.028**	146.0	−2.01	3.425	0.032
G02	53.82	−3.59	1.229	0.034	391.4	−5.74	5.725	**0.031**	214.9	−2.34	3.243	0.036
G03	54.11	−3.70	1.593	0.028	405.6	−5.98	7.791	**0.023**	229.1	−1.47	4.551	0.024
					Spherical collapse halos							
M11	0.0175	2.66	0.006	0.223	0.244	0.27	3.426	**0.043**	0.187	2.57	2.445	0.051
M35	0.0180	1.62	0.030	0.249	0.240	−0.70	3.214	**0.059**	0.185	1.47	2.301	0.061

NOTE.— Col.(1): Object Id. Col.(2)–(5) (1, 3, γ) model (equation 11 and 12) scale radius r_s, scale density ρ_s, inner profile slope γ, and rms scatter of the fit. Col.(6)–(9) Einasto $r^{1/n}$ model half-mass radius $r_{\rm e}$, associated density $\rho_{\rm e}$, profile shape $n_{\rm Ein}$, and rms scatter of the fit. Col.(10)–(13) Prugniel-Simien model scale radius $R_{\rm e}$, scale density ρ' (the spatial density $\rho_{\rm e}$ at $r = R_{\rm e}$ is such that $\rho_{\rm e} = \rho' {\rm e}^{-b}$), profile shape $n_{\rm PS}$, and rms scatter of the fit. Note: The radius and density units do not apply to M11 and M35. For each halo, of the three models shown here the model having the lowest residual scatter is high-lighted in bold.

TABLE 2
THREE PARAMETER MODELS *(cont.)*

Halo Id.	r_s kpc	$\log \rho_s$ $M_\odot$ pc^{-3}	γ'	Δ dex
	Anisotropic Dehnen-McLaughlin (Eq.15)			
	Cluster-sized halos			
A09	722.7	−2.21	0.694	**0.013**
B09	1722.	−3.30	0.880	0.040
C09	207.0	−1.34	0.241	0.047
D12	322.8	−1.95	0.683	0.022
E09	330.4	−2.04	0.669	0.034
F09	193.6	−1.56	0.350	0.036
	Galaxy-sized halos			
G00	20.89	−1.11	0.422	**0.017**
G01	25.88	−1.28	0.568	**0.023**
G02	43.05	−1.60	0.581	**0.027**
G03	30.20	−1.34	0.849	0.024
	Spherical collapse halos			
M11	0.025	4.23	0.00	0.179
M35	0.025	3.21	0.00	0.206

NOTE.— Col.(1): Object Id. Col.(2)–(5) Dehnen-McLaughlin (their equation 46b) scale radius r_s, scale density ρ_s, inner profile slope γ', and rms scatter of the fit. Note: The radius and density units do not apply to M11 and M35. When the rms scatter is lower than the value obtained with the other 3-parameter models, it is given in bold.

TABLE 3
TWO PARAMETER MODELS

Halo Id.	r_s kpc	$\log \rho_0$ $M_\odot$ pc^{-3}	Δ dex	r_s kpc	$\log \rho_s$ $M_\odot$ pc^{-3}	Δ dex	r_s kpc	$\log \rho_s$ $M_\odot$ pc^{-3}	Δ dex
		Burkert			NFW		Isotropic Dehnen-McLaughlin (equation 14)		
					Cluster-sized halos				
A09	114.0	−1.65	0.242	419.8	−3.50	0.042	933.7	−2.43	**0.018**
B09	145.2	−2.23	0.247	527.2	−4.03	0.068	1180.0	−2.97	**0.042**
C09	96.16	−1.74	0.181	284.4	−3.42	**0.042**	554.3	−2.27	0.091
D12	68.39	−1.62	0.230	213.3	−3.34	0.051	409.1	−2.17	**0.026**
E09	77.09	−1.80	0.215	227.0	−3.46	0.053	428.2	−2.28	**0.037**
F09	80.17	−1.85	0.181	229.0	−3.49	**0.030**	438.2	−2.32	0.066
					Galaxy-sized halos				
G00	10.12	−1.56	0.139	22.23	−2.94	**0.024**	34.43	−1.59	0.037
G01	10.28	−1.54	0.152	23.12	−2.95	0.038	36.53	−1.61	**0.031**
G02	14.06	−1.66	0.183	36.39	−3.22	0.044	63.06	−1.96	**0.035**
G03	09.35	−1.32	0.179	19.54	−2.68	0.066	26.98	−1.23	**0.025**
					Spherical collapse halos				
M11	0.0261	3.01	**0.203**	0.0309	2.23	0.233	0.0234	4.31	0.244
M35	0.0265	1.98	**0.231**	0.0314	1.20	0.259	0.0236	3.29	0.269

NOTE.— Col.(1): Object Id. Col.(2)–(4) Burkert (1995) model scale radius r_s, central density ρ_0, and rms scatter of the fit (using $m-2$ in the denominator of equation refEqChi). Col.(5)–(7) NFW (1, 3, 1) model scale radius r_s, scale density ρ_0, and rms scatter of the fit (using $m-2$). Col.(8)–(10) Dehnen-McLaughlin (2005, their equation 20b) model scale radius r_s, associated density ρ_s, and rms scatter (using $m-2$). This model has an inner and outer, negative logarithmic slope of $7/9 \approx 0.78$ and $31/9 \approx 3.44$, respectively. Note: The above radius and density units do not apply to M11 and M35. For each halo, the 2-parameter model with the lowest residual scatter is high-lighted in bold.

4.1.2. *Dehnen-McLaughlin's anisotropic 3-parameter model*

Dehnen & McLaughlin (2005, their equation 46b) present a theoretically-motivated, 3-parameter model such that $[\alpha, \beta, \gamma] = [2(2 - \beta_0)/9, (31 - 2\beta_0)/9, (7 + 10\beta_0)/9]$, and the term β_0 reflects the central ($r = 0$) anisotropy — a measure of the tangential to radial velocity dispersion[1]. Setting $\gamma' = (7 + 10\beta_0)/9$, we have $[\alpha, \beta, \gamma] = [(3 - \gamma')/5, (18 - \gamma')/5, \gamma']$, and their density model can be written as

$$\rho(r) = \frac{2^6 \rho_s}{(r/r_s)^{\gamma'}[1 + (r/r_s)^{(3-\gamma')/5}]^6}, \qquad (15)$$

As shown in Figure 10, for three of the six cluster-sized halos, this model has the greatest residual scatter of the four, 3-parameter models tested here. For another two of the six cluster-sized halos it has the second greatest residual scatter. This model is also unable to match the curvature in the halos of the cold collapse models (Figure 10). However, it does provide very good fits to the galaxy-sized halos, and actually has the smallest residual scatter for three of these halos (Table 2).

The shallowest, inner, negative logarithmic slope of this model occurs when $\beta_0 = 0$, giving a value of $7/9 \approx 0.78$. For non-zero values of β_0, this slope steepens roughly linearly with β_0.

4.2. Sérsic/Einasto model

Sérsic (1963, 1968) generalized de Vaucouleurs' (1948) $R^{1/4}$ light-profile model by replacing the exponent $1/4$ with $1/n$, such that n was a free parameter that measured the 'shape' of a galaxy's light-profile. Using the observers' notion of 'concentration' (see the review in Graham, Trujillo, & Caon 2001), the quantity n is monotonically related to how centrally concentrated a galaxy's light-profile is. With R denoting the *projected* radius, Sérsic's $R^{1/n}$ model is often written as

$$I(R) = I_{\rm e} \exp\left\{-b_n \left[(R/R_{\rm e})^{1/n} - 1\right]\right\}, \qquad (16)$$

where $I_{\rm e}$ is the (projected) intensity at the (projected) effective radius $R_{\rm e}$. The term b_n is not a parameter but a function of n and defined in such a way that $R_{\rm e}$ encloses half of the (projected) total galaxy light (Caon et al. 1993; see also Ciotti 1991, his equation (1)). A good approximation when $n \gtrsim 0.5$ is given in Prugniel & Simien (1997) as

$$b_n \approx 2n - 1/3 + 0.009876/n. \qquad (17)$$

Assorted expressions related to the $R^{1/n}$ model can be found in Graham & Driver's (2005) review article.

Despite the success of this model in describing the light-profiles of elliptical galaxies (e.g., Phillipps et al. 1998; Caon et al. 1993; D'Onofrio et al. 1994; Young & Currie 1995; Graham et al. 1996; Graham & Guzmán 2003, and references therein), it is nonetheless an empirical fitting function with no commonly recognized physical basis. We are therefore free to explore the suitability of this model for describing the mass-density profiles, $\rho(r)$, of dark matter halos. Indeed, Einasto (1965, eq. 4; 1968, eq. 1.7; 1969, eq. 3.1) independently developed the functional form of Sérsic's equation and used it to describe density profiles. More recent application of this model can be found in Einasto & Haud (1989, eq. 14) and Tenjes, Haud, & Einasto (1994, eq. A1). This model has more recently been used in Navarro et al.'s (2004) and Merritt et al.'s (2005) quantification of dark matter halos, and Aceves, Velázquez, & Cruz's (2006) description of the merger remants of simulated disk galaxy collisions.

To avoid potential confusion with Sérsic's $R^{1/n}$ model, we define the following expression as Einasto's $r^{1/n}$ model:

$$\rho(r) = \rho_{\rm e} \exp\left\{-d_n \left[(r/r_{\rm e})^{1/n} - 1\right]\right\}, \qquad (18)$$

where r is the *spatial* (i.e., not projected) radius. The term d_n, defined below, is a function of n such that $\rho_{\rm e}$ is the density at the radius $r_{\rm e}$ which defines a volume containing half of the total mass. The central density is finite and given by $\rho(r = 0) = \rho_{\rm e} {\rm e}^{d_n}$.

The integral of equation (18) over some volume gives the enclosed mass[2], which is also finite and equal to

$$M(r) = 4\pi \int_0^r \left[\rho(\bar{r})\bar{r}^2\right] {\rm d}\bar{r}. \qquad (19)$$

[1] Note: the quantities β and β_0 are not as related as their notation suggests. The former is the outermost, negative logarithmic slope of the density profile while the latter is the velocity anisotropy parameter at $r = 0$.

[2] A similar expression is given in Mamon & Łokas 2005, their equation (A2); and Cardone et al. 2005, their equation (11).

This can be solved by using the substitution $\bar{x} \equiv d_n(\bar{r}/r_{\rm e})^{1/n}$ to give

$$M(r) = 4\pi n r_{\rm e}^3 \rho_{\rm e} {\rm e}^{d_n} {d_n}^{-3n} \gamma(3n, x), \qquad (20)$$

where $\gamma(3n, x)$ is the incomplete gamma function defined by

$$\gamma(3n, x) = \int_0^x {\rm e}^{-t} t^{3n-1} {\rm d}t. \qquad (21)$$

Replacing $\gamma(3n, x)$ with $\Gamma(3n)$ in equation (20) gives the total mass M_{tot}. The circular velocity is simply $v_{\rm circ}(r) = \sqrt{GM(r)/r}$.

The value of d_n, which we first saw in equation (18), is obtained by solving $\Gamma(3n) = 2 \times \gamma(3n, d_n)$, where Γ is the (complete) gamma function. The value of d_n can be well approximated (Mamon 2005, priv. comm.) by the expression

$$d_n \approx 3n - 1/3 + 0.0079/n, \text{ for } n \gtrsim 0.5 \qquad (22)$$

(see Figure 11).

In Paper II we recast Einasto's $r^{1/n}$ model using the radius r_{-2}, where the logarithmic slope of the density profile equals -2.

Einasto's $r^{1/n}$ model (see Einasto & Haud (1989), was used in Navarro et al. (2004; their equation 5) to fit their simulated dark matter halos. They obtained $n \sim 1/(0.172 \pm 0.032) \sim 6 \pm 1.1$. Subsequently, Merritt et al. (2005) showed that Einasto's $r^{1/n}$ model performed as well as the (1, 3, γ) model, and gave better fits for the dwarf- and galaxy-sized halos, obtaining $n \sim 5.6 \pm 0.7$. For a sample of galaxy-sized halos, Prada et al. (2005) obtained similar values of 6 to 7.5.

Figure 12 shows the application of equation (18) to the dark matter density profiles presented in Section 3. A comparison with the (1, 3, γ) model fits in Figure 5 reveals that Einasto's model provides a better description for five of the six cluster-sized halos, three of the four galaxy-sized halos, and both of the spherical collapse halos.

Navarro et al. (2004) wrote "adjusting the parameter [n] allows the profile to be tailored to each individual halo, resulting in improved fits"[3]. Such a breaking of structural homology (see Graham & Colless 1997 for an analogy with projected light-profiles) replaces the notion that a universal density profile may exist.

A number of useful expressions pertaining to Einasto's model, when used as a density profile (equation 18), are given in Cardone et al. (2005) and Mamon & Łokas (2005). In particular, Cardone et al. provide the gravitational potential, as well as approximations to the surface density and space velocity dispersion of the Einasto $r^{1/n}$ model, while Mamon & Lokas give approximations for the concentration parameter, central density, and $M_{\rm virial}/M_{\rm total}$. The nature of the inner profile slope of Einasto's $r^{1/n}$ model and several other useful quantities are presented in Paper II.

4.3. Prugniel-Simien model: A deprojected Sérsic $R^{1/n}$ model

While Merritt et al. (2005) tested how well a numerical deprojection of Sérsic's $R^{1/n}$ model fit their dark matter halo sample, here we test the analytical approximation presented in Prugniel & Simien (1997; their equation B6).

Prugniel & Simien's density model (equation 23), constructed to match deprojected Sérsic $R^{1/n}$ light-profiles, is a generalization of equation (2) in Mellier & Mathez (1987). In equation (23), the exponent p is a function of n, rather than the constant value of 0.855 which is suitable for matching the deprojected form of the $R^{1/4}$ model. In passing we note that the model in Mellier & Mathez was itself a modification of equation (33) from Young (1976), which itself derived from the work of Poveda, Iturriaga, & Orozco (1960) who used $p = 3/4$. The density model in Prugniel & Simien (1997) has been further developed in Terzić & Graham (2005) who derived simple expressions, in terms of elementary and special functions, for the gravitational potential and force. Expressions and diagrams for the spatial and line-of-sight velocity dispersion are also given there.

The accuracy of Prugniel & Simien's (1997) analytical approximation to the deprojection of the Sérsic $R^{1/n}$ model (equation 16) is shown in Figure 13 over the radial range $10^{-2} < r/R_{\rm e} < 10^2$ and for values of n = 0.5, 1, 2, 4, and 10. This

[3]The value of n, equal to $1/\alpha$ in Navarro et al.'s (2004) notation, ranged from 4.6 to 8.2 (Navarro et al. 2004, their table 3).

density model can be written as

$$\rho(r) = \rho' \left(\frac{r}{R_{\rm e}}\right)^{-p} \exp\left[-b\,(r/R_{\rm e})^{1/n}\right], \quad (23)$$

with

$$\rho' = \frac{M}{L}\ I_{\rm e} {\rm e}^b\ b^{n(1-p)}\ \frac{\Gamma(2n)}{2R_{\rm e}\Gamma(n(3-p))}. \quad (24)$$

The parameters $R_{\rm e}$ and n will be recognizable from Sérsic's $R^{1/n}$ model (equation 16). Here, the quantity $R_{\rm e}$ is the half-mass radius of the projected distribution, and n describes the curvature of this projected profile. To the accuracy of Figure 13, this model largely tests how well the *projected* dark matter distribution is described by a Sérsic $R^{1/n}$ model. By construction, the n in this equation is (essentially) the same as the n in Sérsic's $R^{1/n}$ law, equation (16). However, it is *not* equivalent to the n in equation (18).

Although the third parameter ρ' is obtained from fitting the density profile, it can be defined in such a way that the total (finite) mass from equation (23) equals that from equation (16), giving equation (24). For clarity, we have dropped the subscript n from b_n. Like this quantity b (equation 17), the term p is also expressed as a function of n and is given by

$$p = 1.0 - 0.6097/n + 0.05463/n^2 \quad (25)$$

for $0.6 < n < 10$ and $10^{-2} \leq r/R_{\rm e} \leq 10^3$ (Lima Neto et al. 1999)[4]. Setting $p = 0$, the Prugniel-Simien model reduces to the Einasto model. (Although not explored here, by adjusting the value of p in terms of n, one can create a density profile having any desired inner profile slope.)

The density at $r = R_{\rm e}$ is given by $\rho_{\rm e} = \rho' {\rm e}^{-b}$, while the projected surface density at $R = R_{\rm e}$, denoted by $I_{\rm e}$, can be solved for using equation (24). Thus, one can immediately construct (a good approximation to) the projected mass distribution, which will have a Sérsic form (equation 16) with parameters ($R_{\rm e}, I_{\rm e}$, and n).

In Paper II we recast this model using the radius where the logarithmic slope of the density profile equals -2.

[4]The value of p given in equation 25 is preferable to the value $1.0 - 0.6097/n + 0.05563/n^2$ given in Márquez et al. (2000), (Lima Neto 2005, priv.comm.).

The mass profile (Terzić & Graham 2005, their Appendix A; see also Lima Neto et al. 1999 and Márquez et al. 2001), can be written as

$$M(r) = 4\pi\rho' {R_{\rm e}}^3 n b^{n(p-3)} \gamma\left(n(3-p), Z\right), \quad (26)$$

where $Z \equiv b(r/R_{\rm e})^{1/n}$ and $\gamma(a, x)$ is the incomplete gamma function given in equation (21). The total mass is obtained by replacing $\gamma\left(n(3-p), Z\right)$ with $\Gamma\left(n(3-p)\right)$, and the circular velocity is given by $v_{\rm circ}(r) = \sqrt{GM(r)/r}$.

In Figure 14, Equation 23 has been applied to our dark matter profiles. The average ($\pm$ standard deviation) of the shape parameter for the galaxy-sized and cluster-sized halos is $n = 3.59(\pm 0.65)$ and $n = 2.89(\pm 0.49)$, respectively. Merritt et al. (2005, their Table 1) found values of 3.40 ± 0.36 and 2.99 ± 0.49 for their sample of galaxies and clusters, respectively, in good agreement with the results obtained here using a different set of N-body simulations and equation 23, rather than a numerically deprojected $R^{1/n}$ light-profile.

Such non-homology (i.e., different n) makes things more complicated because the question arises as to which density scale and radial scale to use. In the presence of a 'universal' density profile, the difference between the radius $R_{\rm e}$ and r_{-2} (the radius where the logarithmic slope of the density profile equals -2, see Paper II) is a constant factor, but with varying values of n this is not the case. This remark also holds for the scale density, which is used to measure the contrast with the background density of the universe and provide the so-called halo 'concentration'. This then raises the question of what 'concentration' should one actually be using, and if systematic biases exist if one uses ρ_{-2} rather than say $\rho_{\rm e}$. To reiterate this point, the difference in density between $r = r_{-2}$ and $r = R_{\rm e}$ depends on the profile shape n, and thus, apparently, on the halo mass. In Figure 15 we show how the use of r_{-2} and $R_{\rm e}$ produce slightly different results in the size-density diagram (e.g., Navarro et al., their Figure 8). What one can see is that the size (or equivalently mass) dependence on the central concentration (i.e. density) varies depending on how one measures the sizes (and also densities) of the halos.

Figure 14 also reveals that CDM halos resemble galaxies. The projection of the Prugniel-Simien density model closely matches the Sérsic $R^{1/n}$

model (see Terzić & Graham 2005, their figure 4). Subject to vertical and horizontal scaling, CDM halos have similar mass distributions to elliptical galaxies with an absolute B-band magnitude around -18 ± 1 mag; these galaxies have $n \sim 3$ (see Graham & Guzmán 2003, their figure 9). This result has been largely hidden due to the past use of differing empirical models by observers and modelers, until Łokas & Mamon (2001) who found that the projection of an NFW model is well described by a Sérsic $R^{1/n}$ model with $n \sim 3$ — see also Dalcanton & Hogan (2001) who soon after found that the projected NFW resembles the $n = 4$ de Vaucouleurs model — as was recently deduced by Merritt et al.'s (2005) analysis of the halos in cosmological N-body simulations.

Before moving on, we again remark that we have not explored potential refinements to the expression for the quantity p, but note that this could result in a better matching of the model to the simulated profiles from 0.01 to 1 $r_{\rm vir}$. Moreover, in principle, one could also obtain a different inner profile slope (see Paper II), by re-defining the quantity p, in terms of n, subject to the requirement that the global fit remains good.

5. Model comparison: Which did best?

Table 4 summarizes how well each model performed by listing, for each type of halo, the rms value of Δ (equation 10a) for each set of halos, given by

$$\Delta_{\rm rms} = \sqrt{\frac{1}{N}\sum_{i=1}^{N}\Delta_i^2}, \qquad (27)$$

with $N = 6$, 4 and 2 for the cluster-sized, galaxy-sized, and spherical-collapse halos, respectively. A more detailed description of each model's performance follows.

The bowl- and hump-shaped residual profiles associated with the 2-parameter model of Burkert (1995) reveal this model's inability to describe the radial mass distribution in our simulated dark matter halos. The 2-parameter model of Dehnen & McLaughlin (2005) performs considerably better, although it too fails to describe the cold collapse systems and two of the six cluster-sized halos, specifically C09 and F09. Although this (4/9, 31/9, 7/9) model never provides the best fit, it does equal or out-perform the NFW-like (1, 3, γ) model in describing 3 of the 12 halos (A09, D12, G03).

In general, all of the 3-parameter models perform well ($0.015 \lesssim \Delta \lesssim 0.04$ dex) at fitting the N-body (non-collapse) halos. However, neither the (1, 3, γ) model nor the 3-parameter Dehnen-McLaughlin model can match the curvature in the density profiles of the cold collapse systems (M11 & M35). On the other hand, both Einasto's $r^{1/n}$ model and that from Prugniel & Simien give reasonably good fits ($\Delta \sim 0.05$ dex) for these two monolithic collapse halos.

The Prugniel-Simien model provided the best overall description of the cluster-sized, N-body halos. The (1, 3, γ) model and the 3-parameter Dehnen-McLaughlin model provided the best fit for only one cluster-sized, N-body halo each, and even then the (1, 3, γ) model only just outperformed the Prugniel-Simien model which gave the best fit for four of the six cluster-sized halos. For two of these halos, the size of the residual about the optimal Prugniel-Simien fit was roughly half of the value obtained when using the (1, 3, γ) model.

The implication of this result is that Sérsic's $R^{1/n}$ model will describe the projected surface density of the cluster-sized, dark matter halos. Intriguingly, Demarco et al. (2003) and Durret, Lima Neto & Forman (2005) have observed that the (projected) hot X-ray gas distribution in clusters can indeed be described with Sérsic's $R^{1/n}$ model; although the gas can at times display a rather unrelaxed behavior (Statler & Diehl 2006). Studies of gravitational lensing may therefore benefit from the use of Sérsic's $R^{1/n}$ model for which the lensing equation has been solved (Cardone et al. 2004) and for which numerous other properties have previously been computed (Graham & Driver 2005).

With regard to the galaxy-sized, N-body halos, the situation is somewhat different. Dehnen & McLaughlin's (2005) anisotropic 3-parameter model provided the best fit for three of the four profiles, with the Einasto $r^{1/n}$ model providing the best fit for the forth profile. We also observe that Einasto's model provided better fits than the (1, 3, γ) model for three of the four N-body halos. If this observation holds, namely, that the Prugniel-Simien model describes the density profiles of the cluster-sized halos best, while Dehnen

& McLaughlin's 3-parameter model provides the best description of the galaxy-sized halos, it would imply that these halos do not have the same structural form. Of course, even if the same model *did* provide the best fit for both types of halo, any variation in the value of the profile shape n, or central isotropy parameter β_0, would point toward the existence of nonhomology.

Figure 16 shows our N-body halos, together with real elliptical galaxies and clusters, in the profile shape vs. mass plane. The profile shape parameter plotted there is either n from the Sérsic $R^{1/n}$ model fit to the light profile, or the corresponding parameter from the Prugniel-Simien model fit to the dark-matter density. Dynamical masses from the Demarco et al. (2003) study of galaxy clusters are shown. We have also included the elliptical galaxy compilation in Graham & Guzmań (2003), converting their B-band luminosities into solar masses using a stellar mass-to-light ratio of 5.3 (Worthey 1994, for a 12 Gyr old SSP), and an absolute B-band magnitude for the Sun of 5.47 B-mag (Cox 2000). This approach ignores the contribution from dark matter in galaxies. However, given the uncertainties on how $M_{\rm tot}/L$ varies with L (e.g., Trujillo, Burkert, & Bell 2004, and references therein) we prefer not to apply this correction, and note that the galaxy masses in Figure 16 only reflect the stellar mass. Figure 16 suggests that the simulated galaxy-sized halos have a different shape parameter, i.e. a different mass distribution, than the simulated cluster-sized halos.

The same conclusion was reached by Merritt et al. (2005) who studied a different sample of N-body halos. The sample of dwarf- and galaxy-sized halos from that paper had a mean (± standard deviation)[5] profile shape $n = 3.04(\pm 0.34)$, while the cluster-sized halos had $n = 2.38(\pm 0.25)$. We observe this same systematic difference in our N-body halos. Taking the profile shape n from the Prugniel-Simien model fits to the density profile (equivalent to the value of n obtained by fitting Sérsic's $R^{1/n}$ model to the projected distribution) we find $n = 3.59(\pm 0.65)$ for our cluster-sized halos and $n = 2.89(\pm 0.49)$ for our galaxy-sized halos. A Student t test, without assuming equal variance in the two distributions, reveals the above means are different at the 88% level. Applying the same test to the data of Merritt et al. (2005; their Table 1, column 2), which is double the size of our sample and also contains dwarf galaxy-sized halos, we find that the means are different at the 99.98% level. We conclude that there is a significant mass dependence in the density profiles of simulated dark-matter halos. Density profiles of more massive halos exhibit more curvature (smaller n) on a log-log plot.

To better explore how the homology (i.e., universality) of CDM halos is broken, it would be beneficial to analyze a large, low-resolution sample of halos from a cosmological cube simulation in order to obtain good statistics. Moreover, the collective impact from differing degrees of virialization in the outer regions, possible debris wakes from larger structures, global ringing induced by the last major merger, triaxiality, and the presence of large subhalos could be quantified.

6. Summary

We have compared the ability of three 2-parameter models and four 3-parameter models to describe the density profiles of a sample of simulated, dark matter halos. Rather than simply binning the halo particles into concentric shells, the density profiles were constructed assuming that the particles represent a random sample drawn from the underlying density. Smooth estimates of the "true" density profiles were extracted from the N-body data using techniques from nonparametric function estimation theory, and these estimates were compared with the parametric models to determine the best-fit parameters of the latter, and the relative quality of the parametric fits.

Not surprisingly, the 3-parameter models were found to perform better than the 2-parameter models of Burkert (1995), Navarro et al. (1995), and Dehnen & McLaughlin (2005). Over the fitted radial range $0.01 \lesssim r/r_{\rm vir} < 1$, both the Einasto $r^{1/n}$ model (identical to Sérsic's model if the latter is expressed in terms of space, rather than projected density) and the Prugniel-Simien model (an analytical approximation to a de-projected Sérsic law) provide a better description of the data than the (1, 3, γ) model, i.e. the NFW-like double power-law model with inner slope γ. Moreover,

[5]Reminder: the uncertainty on the mean is not equal to the standard deviation.

TABLE 4

RESIDUAL SCATTER: RMS VALUES OF Δ.

Model	Cluster-sized halos	Galaxy-sized halos	Spherical-collapse halos
	3-parameter models		
Einasto	**0.028**	**0.026**	**0.052**
Prugniel-Simien	**0.025**	0.030	**0.056**
$(1, 3, \gamma)$	0.032	0.028	0.236
Dehnen-McLaughlin (Eq.15)	0.034	**0.023**	0.193
	2-parameter models		
Dehnen-McLaughlin (Eq.14)	0.053	0.032	0.257
NFW	0.046	0.046	0.246
Burkert	0.218	0.164	0.217

NOTE.— Col.(1): Model. Col.(2): rms of the 6 residual scatters, $\Delta_{\rm rms}$ (equation 27), for the cluster-sized halos. Col.(3): Similar to Col.(2) but for the 4 galaxy-sized halos. Col.(3): Similar to Col.(2) but for the 2 spherical collapse halos. For each halo type, the two models which perform the best are highlighted in bold.

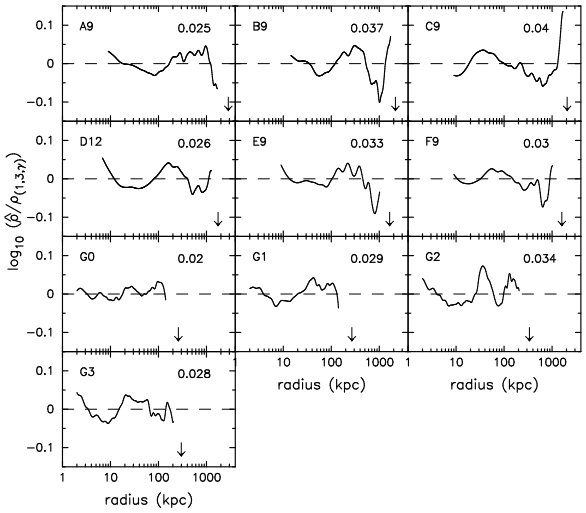

Fig. 5.— Residual profiles from application of the 3-parameter (1, 3, γ) model (equation 12) to our ten, N-body density profiles. The virial radius is marked with an arrow, and the rms residual (equation 10a) is inset with the residual profiles.

unlike the (1, 3, γ) model, both of these models have finite total mass, and are also capable of describing the density profiles of halos formed from the cold collapse of a spherical over-density (Figure 6).

The single function that provides the best overall fit to the halo density profiles is Einasto's law, equation (18):

$$\rho(r) = \rho_{\rm e} \exp\left\{-d_n \left[(r/r_{\rm e})^{1/n} - 1\right]\right\}$$

with d_n defined as in equation (22). This conclusion is consistent with that of an earlier study (Merritt et al. 2005) that was based on a different set of N-body halos. Typical values of the "shape" parameter n in equation (18) are $4 \lesssim n \lesssim 7$ (Table 1). Corresponding n values from Sérsic profile fits to the projected (surface) density range from ~ 3 to ~ 3.5 (Fig. 16).

We propose that Einasto's model, equation (18), should be more widely used to characterize the density profiles of N-body halos. As noted above, Einasto's model has already found application in a number of observationally-motivated studies of the distribution of mass in galaxies and galaxy clusters.

While equation (18) is a good description of all of the halo models considered here, we found that systematic differences do exist in the best-

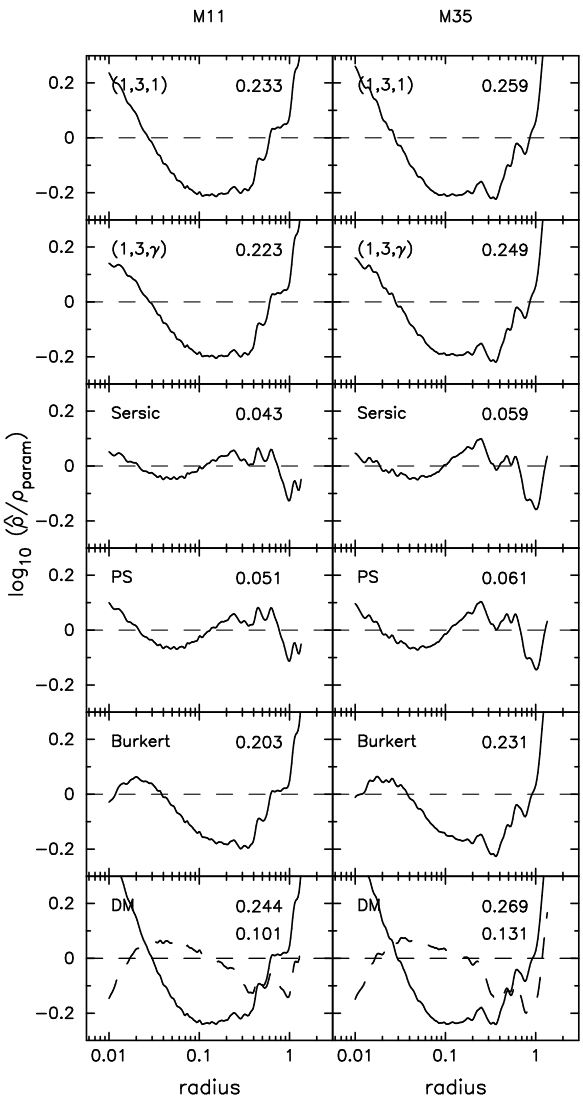

Fig. 6.— Residual profiles from the application of seven different parametric models (see Section 4) to our "cold collapse" density halos, M11 and M35. Einasto's model, which has the same functional form as Sérsic's model, is labelled 'Sersic' in this Figure. In the lower panel, the solid curve corresponds to the 2-parameter model from Dehnen & McLaughlin (2005), and the dashed curve corresponds to their 3-parameter model. The rms residual (equation 10a) is inset in each figure.

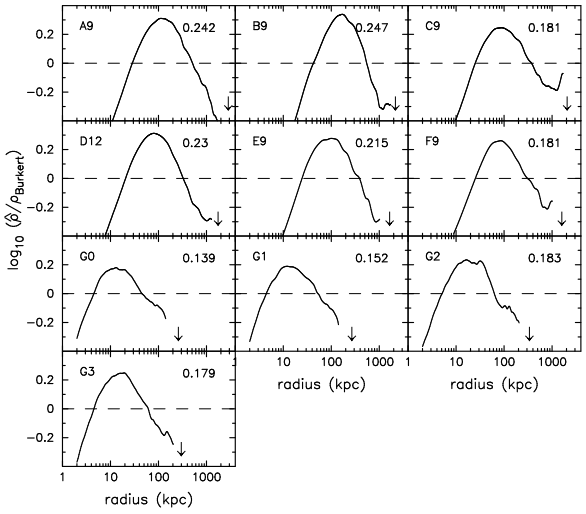

Fig. 7.— Residual profiles from application of Burkert's 2-parameter model (equation 13) to our dark matter density profiles.

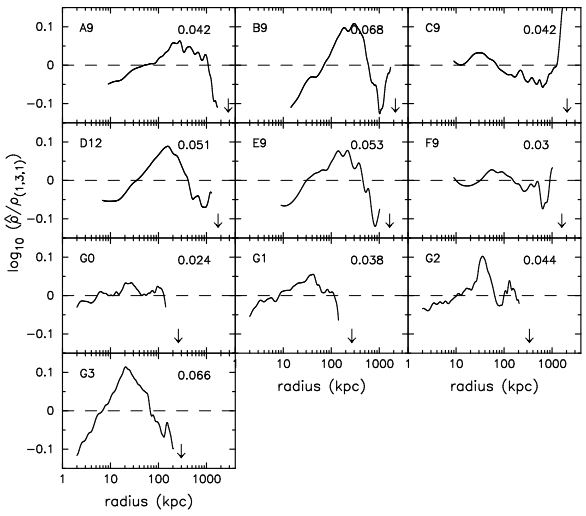

Fig. 8.— Residual profiles from application of the 2-parameter NFW (1, 3, 1) model to our dark matter density profiles.

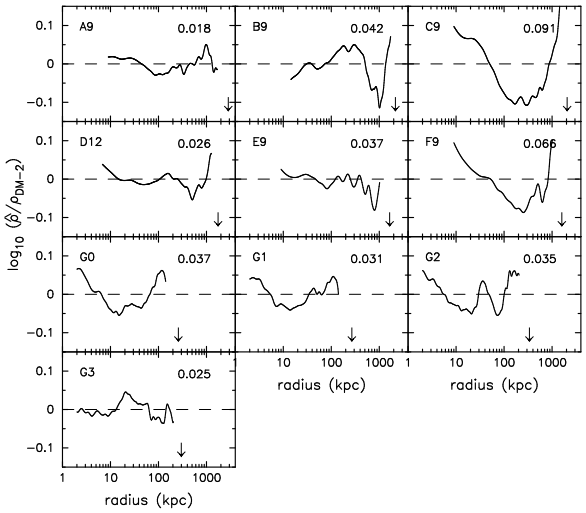

Fig. 9.— Residual profiles from application of the 2-parameter (4/9, 31/9, 7/9) model (equation 14) from Dehnen & McLaughlin (2005, their equation 20b) to our dark matter density profiles.

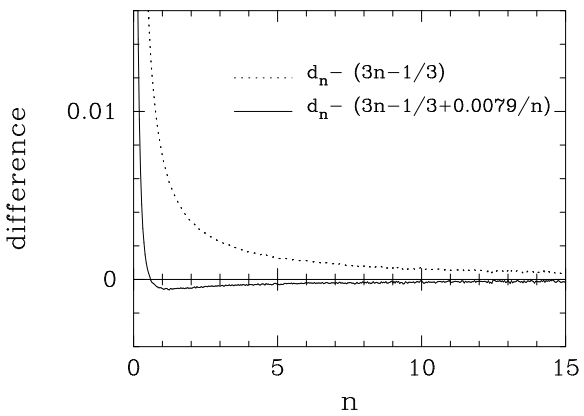

Fig. 11.— Difference between the exact value for d_n from equation (18), such that $\Gamma(3n) = 2\gamma(3n, d_n)$, and the two approximations inset in the Figure.

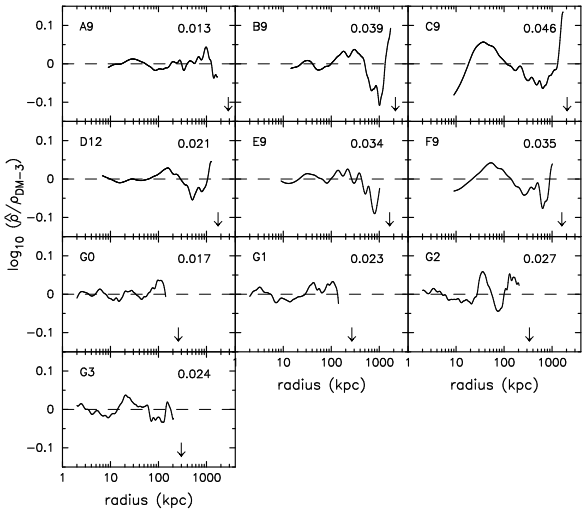

Fig. 10.— Residual profiles from application of the 3-parameter $[(3-\gamma')/5, (18-\gamma')/5, \gamma']$ model (equation 15) from Dehnen & McLaughlin (2005, their equation 46b) to our dark matter density profiles.

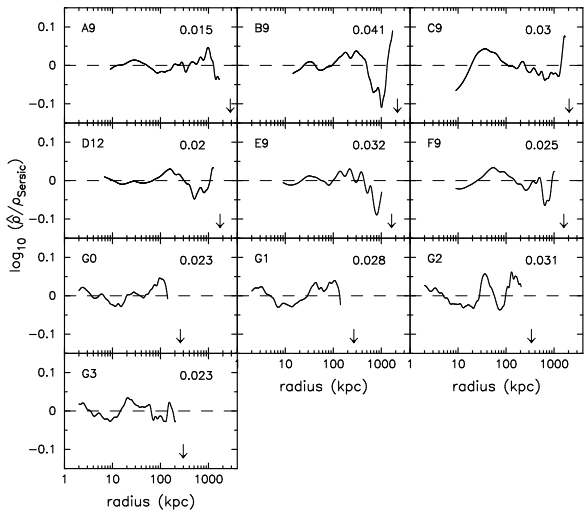

Fig. 12.— Residual profiles from application of Einasto's $r^{1/n}$ model (equation 18) to our dark matter density profiles.

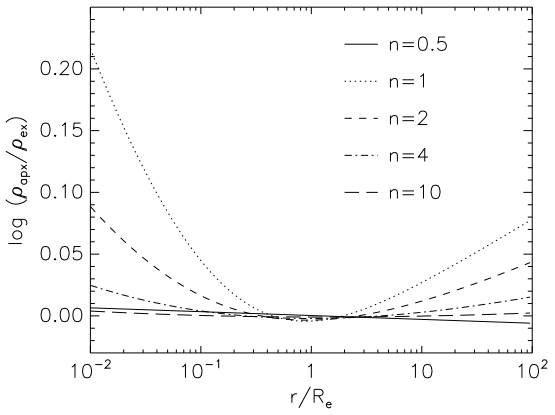

Fig. 13.— Logarithmic difference between the exact deprojection of Sérsic's $R^{1/n}$ model (equation 16) and the approximation given by Prugniel & Simien (1997) in equation (23), using the values of p and b given in equations (25) and (17), respectively.

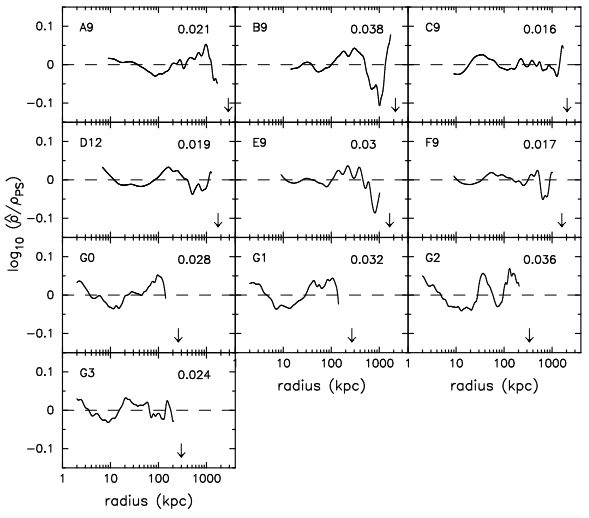

Fig. 14.— Residual profiles from application of the Prugniel & Simien model (equation 23) to our dark matter density profiles.

fit models that describe N-body halos formed via hierarchical merging on the one hand, and those formed via spherical collapse on the other hand, in the sense that the latter have substantially smaller shape parameters, $n \approx 3.3$ (Table 1). That is, the density profiles in the cold collapse halos decline more quickly than r^{-3} at large radii, and have shallower inner profile slopes than those produced in simulations of hierarchical merging.

With regard just to the non-collapse models, we also found systematic differences between the cluster- and galaxy-sized halos. The latter are slightly better fit by the 3-parameter Dehnen-McLaughlin model, and the former are slightly better fit by the Prugniel-Simien model (Table 4). This, together with the observation that more massive halos tend to have smaller shape parameters n (Figure 16), suggests that there may not be a truly "universal" density profile that describes ΛCDM halos.

We kindly thank Gary Mamon for his detailed comments on this manuscript. We are additionally grateful to Walter Dehnen and Dean McLaughlin for their helpful corrections and comments. We also wish to thank Peeter Tenjes for tracking down and kindly faxing us copies of Einasto's original papers in Russian. A.G. acknowledges support from NASA grant HST-AR-09927.01-A from the Space Telescope Science Institute. D.M. was supported by grants AST 04-20920 and AST 04-37519 from the National Science Foundation and grant NNG04GJ48G from NASA. J.D. is grateful for financial support from the Swiss National Science Foundation. B.T. acknowledges support from Department of Energy grant G1A62056.

REFERENCES

Aarseth, S.J. 1963, MNRAS, 126, 223

Aceves, H., Velázquez, H., & Cruz, F. 2006, MNRAS, submitted (astro-ph/0601412)

Aguilar, L.A., & Merritt, D. 1990, ApJ, 354, 33

Austin, C.G., Williams, L.L.R., Barnes, E.I., Babul, A., & Dalcanton, J.J. 2005, ApJ, 634, 756

Bertschinger, E. 1985, ApJS, 58, 39

Binggeli, B., & Jerjen, H. 1998, A&A, 333, 17

Binney, J. J. 1982, MNRAS, 200, 951

Burkert, A. 1995, ApJ, 447, L25

Caon, N., Capaccioli, M., & D'Onofrio, M. 1993, MNRAS, 265, 1013

Cardone, V.F. 2004, A&A, 415, 839

Cardone, V.F., Piedipalumbo, E., & Tortora, C. 2005, MNRAS, 358, 1325

Ciotti, L. 1991, A&A, 249, 99

Cox, D.P. 2000, Allen's Astrophysical quantities, New York: AIP Press; Springer

Dalcanton, J.D., & Hogan, C.J. 2001, ApJ, 561, 35

Dehnen, W., & McLaughlin, D.E. 2005, MNRAS, 363, 1057

Demarco, R., Magnard, F., Durret, F., & Márquez, I. 2003, A&A, 407, 437

de Vaucouleurs, G. 1948, Ann. d'astrophys., 11, 247

Diemand, J., Moore, B., & Stadel, J. 2004a, MNRAS, 352, 535

Diemand, J., Moore, B., & Stadel, J. 2004b, MNRAS, 353, 624

D'Onofrio, M., Capaccioli, M., & Caon, N. 1994, MNRAS, 271, 523

Dubinski, J., & Carlberg, R. 1991, ApJ, 378, 496

Durret, F., Lima Neto, G.H., & Forman, W. 2005, A&A, 432, 809

Efstathiou, G.P., Frenk, C.S., White, S.D.M., & Davis, M. 1988, MNRAS, 235, 715

Einasto, J. 1965, Trudy Inst. Astrofiz. Alma-Ata, 5, 87

Einasto, J. 1968, Tartu Astr. Obs. Publ. Vol. 36, Nr 5-6, 414,

Einasto, J. 1969, Astrofizika, 5, 137

Einasto, J., & Haud, U. 1989, A&A, 223, 89

Eke, V.R., Cole, S., & Frenk, C.S. 1996, MNRAS, 282, 263

Fillmore, J.A., & Goldreich, P. 1984, ApJ, 281, 1

Flores, R.A., & Primack, J.R. 1994, ApJ, 427, L1

Frenk, C.S., White, S.D.M., Davis, M., & Efstathiou, G.P. 1988, ApJ, 327, 507

Graham, A.W., & Colless, M.M. 1997, MNRAS, 287, 221

Graham, A.W., & Driver, S. 2005, PASA, 22(2), 118

Graham, A.W., Erwin, P., Trujillo, I., & Asensio Ramos, A. 2003, AJ, 125, 2951

Graham, A.W., & Guzmán, R. 2003, AJ, 125, 2936

Graham, A.W., Lauer, T., Colless, M.M., & Postman, M. 1996, ApJ, 465, 534

Graham, A.W., Merritt, D., Moore, B., Diemand, J., & Terzić, B. 2006a, AJ, submitted (Paper II)

Graham, A.W., Merritt, D., Moore, B., Diemand, J., & Terzić, B. 2006b, AJ, submitted (Paper II)

Graham, A.W., Trujillo, N., & Caon, N. 2001, AJ, 122, 1707

Hansen, S.H., & Moore, B. 2006, New Astronomy, 11, 333

Hénon, M. 1964, Annales d'Astrophysique, 27, 83

Hernquist, L. 1990, ApJ, 356, 359

Hoffman, Y. 1988, ApJ, 328, 489

Jaffe, W. 1983, MNRAS, 202, 995

Jing, Y.P., & Suto, Y. 2000, ApJ, 529, L69

Klypin, A., Kravtsov, A.V., Bullock, J.S., & Primack, J.R. 2001, ApJ, 554, 903

Kravtsov, A.V., Klypin, A.A., Bullock, J.S., & Primack, J.R. 1998, ApJ, 502, 48

Lima Neto, G.B., Gerbal, D., & Márquez, I. 1999, MNRAS, 309, 481

Łokas, E.L., & Mamon, G.A. 2001, MNRAS, 321, 155

Mamon, G.A., & Łokas, E.L. 2005, MNRAS, 362, 95

Mamon, G.A., & Łokas, E.L., Dekel, A., Stoehr, F., & Cox, T.J. 2006, in the 21st IAP meeting, Mass Profiles and Shapes of Cosmological Structures, ed. G.A. Mamon, F. Combes, C. Deffayet & B. Fort (Paris: EDP) (astro-ph/0601345)

Márquez, I., Lima Neto, G.B., Capelato, H., Durret, F., & Gerbal, D. 2000, 353, 873

Márquez, I., Lima Neto, G.B., Capelato, H., Durret, F., Lanzoni, B., & Gerbal, D. 2001, A&A, 379, 767

Mellier, Y., & Mathez, G. 1987, A&A, 175, 1

Merritt, D. 1996, AJ, 111, 2462

Merritt, D., & Aguilar, L. A. 1985, MNRAS, 217, 787

Merritt, D., Navarro, J.F., Ludlow, A., & Jenkins, A. 2005, ApJL, 624, L85

Merritt, D., Tremaine, S. & Johnstone, D. 1989, MNRAS, 236, 829

Merritt, D., & Tremblay, B. 1994, AJ, 108, 514

Moore, B. 1994, Nature, 370, 629

Moore, B., Governato, F., Quinn, T., Stadel, J., & Lake, G. 1998, ApJ, 499, L5

Moore, B., Quinn, T., Governato, F., Stadel, J., & Lake, G. 1999, MNRAS, 310, 1147

Navarro, J.F., Frenk, C.S., & White, S.D.M. 1995, MNRAS, 275, 720

Navarro, J.F., et al. 2004, MNRAS, 349, 1039

Peebles, P.J.E. 1970, AJ, 75, 13

Davies, J.I., Phillipps, S., Cawson, M.G.M., Disney, M.J., & Kibblewhite, E.J. 1988, MNRAS, 232, 239

Pignatelli, E., & Galletta, G. 1999, A&A, 349, 369

Poveda, A., Iturriaga, R., & Orozco, I. 1960, Bol. Obs. Tonantzintla y Tacubaya 2, No.20, p.3

Prada, F., Klypin, A.A., Simonneau, E., & Betancort Rijo, J. 2005, (astro-ph/0506432)

Prugniel, Ph., & Simien, F. 1997, A&A, 321, 111

Rasia, E., Tormen, G., & Moscardini, L. 2004, MNRAS, 351, 237

Reed, D., et al. 2005, MNRAS, 357, 82

Scott, D.W. 1992, Multivariate Density Estimation, Wiley, New York

Sérsic, J.-L. 1963, Boletin de la Asociacion Argentina de Astronomia, vol.6, p.41

Sérsic, J.L. 1968, Atlas de galaxias australes

Silverman, B.W. 1986, Density Estimation for Statistics and Data Analysis (Chapman and Hall: London)

Spergel, D.N. 2003, ApJS, 148, 175

Stadel, J. 2001, PhD thesis, Univ. of Washington

Statler, T.S., & Diehl, S. 2006, BAAS, 207, 178.07

Stepanas, P.G., & Saha, P. 1995, MNRAS, 272, L13

Stiavelli, M., Miller, B.W., Ferguson, H.C., Mack, J., Whitmore, B.C., & Lotz, J.M. 2001, AJ, 121, 1385

Tenjes, P., Haud, U., & Einasto, J. 1994, A&A, 286, 753

Terzić, B., & Graham, A.W. 2005, MNRAS, 362, 197

Trujillo, I., Burkert, A., & Bell, E.F. 2004, ApJ, 600, 39

van Albada, G.B. 1961, AJ, 66, 590

van Albada, T.S. 1982, MNRAS, 201, 939

West, M.J., Dekel, A., Oemler, A., Jr. 1987, ApJ, 316, 1

Worthey, G. 1994, ApJS, 95, 107

Young, P.J. 1976, AJ, 81, 807

Young, C.K., & Currie, M.J. 1995, MNRAS, 273, 1141

Zhao, H.S. 1996, MNRAS, 278, 488

This 2-column preprint was prepared with the AAS LaTeX macros v5.0.

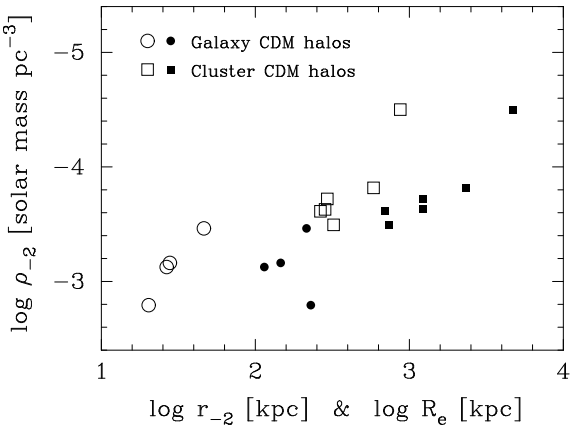

Fig. 15.— The density, ρ_{-2}, where the logarithmic slope of the density profile equals -2 is plotted against i) the radius where this occurs (open symbols), and ii) the effective radius (filled symbols) derived from the best-fitting Prugniel-Simien model (equation 23). Both ρ_{-2} and r_{-2} are also computed from the best-fitting Prugniel-Simien model, see Paper II. If a universal profile existed for these halos, then the vertical difference should be constant for all halos.

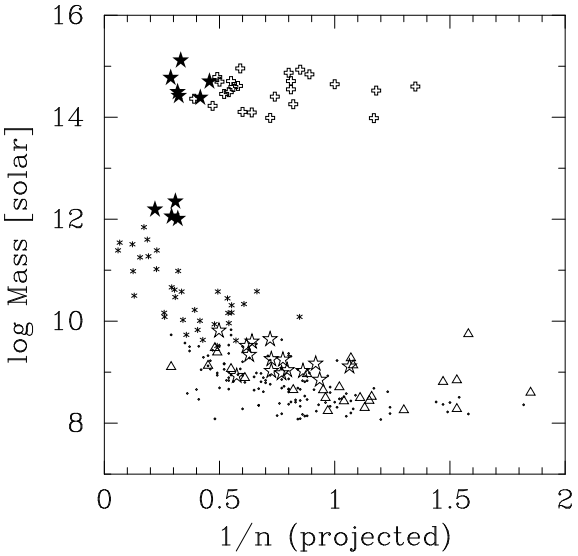

Fig. 16.— Mass versus profile shape ($1/n$). For the galaxies and galaxy clusters, the shape parameters n have come from the best-fitting Sérsic $R^{1/n}$ model to the (projected) light- and X-ray profiles, respectively. The galaxy stellar masses, and cluster gas masses are shown here. For DM halos, the virial masses are shwon and the shape parameters have come from the best-fitting Prugniel-Simien model. (Note: The value of $1/n$ from the Prugniel-Simien model applied to a density profile is equivalent to the value of n from Sérsic's model applied to the projected distribution.) We are plotting baryonic properties for the galaxies alongside dark matter properties for the simulated halos. Filled stars: N-body, dark matter halos from this paper; open plus signs: galaxy clusters from Demarco et al. (2003); dots: dwarf Elliptical (dE) galaxies from Binggeli & Jerjen (1998); triangles: dE galaxies from Stiavelli et al. (2001); open stars: dE galaxies from Graham & Guzmán (2003); asterix: intermediate to bright elliptical galaxies from Caon et al. (1993) and D'Onofrio et al. (1994).